Improvement of convergence to steady state solutions of Euler equations with weighted compact nonlinear schemes

Shuhai Zhang[1], Xiaogang Deng[2], Meiliang Mao[3] and Chi-Wang Shu[4]

Abstract

The convergence to steady state solutions of the Euler equations for weighted compact nonlinear schemes (WCNS) [Deng X. and Zhang H. (2000), J. Comput. Phys. 165, 22-44 and Zhang S., Jiang S and Shu C.-W. (2008), J. Comput. Phys. 227, 7294-7321] is studied through numerical tests. Like most other shock capturing schemes, WCNS also suffers from the problem that the residue can not settle down to machine zero for the computation of the steady state solution which contains shock waves but hangs at the truncation error level. In this paper, the techniques studied in [Zhang S. and Shu. C.-W. (2007), J. Sci. Comput. 31, 273-305 and Zhang S., Jiang S and Shu. C.-W. (2011), J. Sci. Comput. 47, 216-238], to improve the convergence to steady state solutions for WENO schemes, are generalized to the WCNS. Detailed numerical studies in one and two dimensional cases are performed. Numerical tests demonstrate the effectiveness of these techniques when applied to WCNS. The residue of various order WCNS can settle down to machine zero for typical cases while the small post-shock oscillations can be removed.

Key Words: weighted compact schemes, convergence to steady state solution, nonlinear weights

[1]State Key Laboratory of Aerodynamics, China Aerodynamics Research and Development Center, Mianyang, Sichuan 621000, China. E-mail: zhang_shuhai@tom.com. Research supported by the Chinese National Natural Science Foundation grants 11172317, 91016001 and 973 program 2009CB724104.

[2]State Key Laboratory of Aerodynamics, China Aerodynamics Research and Development Center, Mianyang, Sichuan 621000, China. Research supported by 973 program 2009CB723800.

[3]China Aerodynamics Research and Development Center, Mianyang, Sichuan 621000, China. Research supported by 973 program 2009CB723800.

[4]Division of Applied Mathematics, Brown University, Providence, RI 02912, USA. E-mail: shu@dam.brown.edu. Research supported by AFOSR grant FA9550-09-1-0126 and NSF grants DMS-0809086 and DMS-1112700.

1 Introduction

In this paper we study the steady state convergence of weighted compact schemes. Such schemes are combinations of weighted essentially non-oscillatory (WENO) schemes and compact schemes.

WENO schemes were first proposed by Liu et al. [11]. It is an extension of the essentially non-oscillatory (ENO) schemes introduced by Harten et al. [7]. Using a cell average approach (finite volume framework), Liu et al. [11] converted an r-th order ENO scheme to an $(r+1)$-th order WENO scheme. Based on the pointwise finite difference ENO scheme [15, 16] and by a careful design of the smoothness indicator used in the nonlinear weights, the WENO scheme in [9] can achieve the optimal $(2r-1)$-th order accuracy when converting an r-th order ENO scheme, while still keeping the essentially non-oscillatory property near shock waves.

Even though the order of accuracy for explicit finite difference WENO schemes can be designed to be arbitrarily high, such as the eleventh order WENO scheme developed by Balsara and Shu [2], the resolution of short waves of such high order explicit finite difference schemes is still not ideal.

Based on the cell-centered compact scheme proposed by Lele [10], Deng and Zhang [6] developed a class of weighted compact nonlinear schemes (WCNS) using the idea of WENO interpolation for the conservative variables. Instead of the conservative variables, Zhang et al. [19] extended WCNS to higher order weighted compact schemes by a direct weighted interpolation of the flux on the cell interface. The resulted flux type WCNS has similar formulae to those of the regular WENO schemes. Hence, the detailed analysis and even many pieces of the code can be directly copied from those of the regular WENO schemes.

Compared with the regular WENO schemes, WCNS has the same ability to capture strong discontinuities, while the resolution of short waves is improved and numerical dissipation is reduced [19].

The WENO and WCNS schemes are high order finite difference schemes which can

capture strong discontinuities. They have been extensively applied to various multi-scale problems such as shock-turbulence interaction [1], shock induced vortex breakdown [22], aeroacoustics [23] as well as the flow over complex configuration [5].

However, there are still issues that should be studied. One of the most interesting issues is the convergence to steady state solutions, given by the equation

$$\sum_{i=1}^{d} \frac{\partial F_i(U)}{\partial x_i} = 0 \tag{1.1}$$

where U is the vector of the conservative variables, $F_i(U)$ is the (usually nonlinear) flux function in the i-th direction, and d is the spatial dimension. It can be achieved by the time marching method that solves the solution of the time-dependent equation

$$\frac{\partial U}{\partial t} + \sum_{i=1}^{d} \frac{\partial F_i(U)}{\partial x_i} = 0. \tag{1.2}$$

When the time derivative $\frac{\partial U}{\partial t}$ approaches zero, or equivalently when the residue of the numerical scheme approaches machine zero, the steady state solution of the equation (1.1) is obtained. The key of this method is the convergence of the computational procedure which means that the residue should decrease to machine zero.

However, when there are strong discontinuities, which are common in supersonic flows, the residue of shock capturing schemes often cannot settle down to machine zero but will stop at the truncation error level, far above machine zero [17, 21]. Numerical tests show that this difficulty is related to the slight post shock oscillations [17, 21]. Even though there has been a debate on the importance of driving the residue to machine zero, as the numerical error will still be at the truncation error level anyway, these slight post shock oscillations are however troublesome under a few scenarios. First, for multi-scale flows such as supersonic turbulence and shock associated noise, these post-shock oscillations may be confused with the multi-scale feature such as aeroacoustic character and the fluctuation of turbulence. The amplitude of the shock-associated noise may be smaller than the numerical post-shock oscillation. For instance, the radiated pressure fluctuation is less than 10^{-4} for the "terrifyingly loud" noise of $114dB$ of turbo-jets [4], which is smaller than the slight numerical post-shock oscillation

for a Mach 2 steady shock wave. Second, there are a lot of local unsteady flow features such as the shock boundary layer interaction, shock vortex interaction, etc. Such interactions will often result in a locally unsteady movement of the shock wave, which may be confused by the unsteady movement resulted from the post-shock numerical oscillation. In many cases, it is difficult to distinguish between the self-induced unsteady behavior and the artificial unsteady behavior resulted from the post-shock numerical oscillations. Third, when one uses the time marching method to solve the unsteady equation to approach the steady state solution, the residue is often used as a criterion to stop the computation. If the residue refuses to approach machine zero or a value small enough, one can no longer use the size of the average residue to determine when to stop the computation, and must rely on experience including a visual comparison of the flow variables after many time steps to make this determination.

In previous work [21, 20], we proposed two techniques to improve the convergence of the WENO scheme to steady state solutions. The first technique [21] is a new smoothness indicator. By a detailed analysis, we found that the traditional smoothness indicator is not adequate in the near region of the steady shock wave. Hence, we proposed a new smoothness indicator that is better in this region. In the second approach [20], we found that the Roe average procedure used in the local characteristic projection can influence the convergence history. Hence, we used upwind biased interpolations instead of the Roe average in this projection. Both of these techniques can result in the residue settling down to machine zero for many one and two dimensional test cases.

In this paper, we generalize these two techniques to the WCNS schemes, with the objective of testing and comparing the convergence performance of these techniques for steady state solutions. Typical one and two dimensional test cases are given. Numerical results demonstrate that the residue can reach machine zero with these two techniques in many test cases.

The paper is organized as follows. In the second section, we give a brief overview of the methodology of the WCNS schemes and the traditional method to compute the eigenvectors.

In section 3, we describe the generalization of the two techniques to improve the convergence performance to steady states. Section 4 contains our numerical tests and comparisons. The last section is our conclusion.

2 Methodology of WCNS

In this section, we give a brief overview of the finite difference WCNS schemes including the construction of WCNS, smoothness indicator, flux splitting and the discretization of the time derivative.

2.1 Construction of WCNS

We consider numerical approximations to the solution of the scalar conservation law

$$\frac{\partial u}{\partial t} + \frac{\partial f(u)}{\partial x} = 0. \tag{2.1}$$

A semidiscrete finite difference scheme can be written as

$$\frac{\partial u_i}{\partial t} = -f_i' \tag{2.2}$$

where f_i' is the approximation to the spatial derivative of the physical flux $f(u)$ at the grid node x_i. In WCNS, this approximation is computed by a combination of the linear cell-centered compact scheme proposed by Lele [10] and the WENO interpolation [19, 14].

The linear cell-centered compact scheme proposed by Lele [10] has the following form

$$\beta f_{i-2}' + \alpha f_{i-1}' + f_i' + \alpha f_{i+1}' + \beta f_{i+2}' = c\frac{f_{i+\frac{5}{2}} - f_{i-\frac{5}{2}}}{5\triangle x} + b\frac{f_{i+\frac{3}{2}} - f_{i-\frac{3}{2}}}{3\triangle x} + a\frac{f_{i+\frac{1}{2}} - f_{i-\frac{1}{2}}}{\triangle x}. \tag{2.3}$$

The left hand side contains the spatial derivatives f_i' at the grid nodes and the right hand side contains the cell-centered value $f_{i+\frac{1}{2}}$ at the center $x_{i+\frac{1}{2}} = \frac{1}{2}(x_i + x_{i+1})$ of a cell $x \in [x_i, x_{i+1}]$. The constraints on the coefficients α, β, a, b and c correspond to different orders of accuracy that can be derived by matching the Taylor series coefficients and have been listed in the literature [10].

Unlike the WENO scheme [11, 9], which is an explicit numerical scheme, the linear compact scheme given by the equation (2.3) is implicit. It is necessary to solve a five diagonal linear system to obtain the solution of the spatial derivatives f'_i.

There are many methods to compute the value on a cell center $f_{i+\frac{1}{2}}$. For example, Lele [10] proposed a linear compact method. However, this linear method could not capture strong discontinuities. To compute strong discontinuities in fluids, WCNS adopted the idea of WENO interpolation [19, 14] to compute $f_{i+\frac{1}{2}}$ from the values on a stencil. In general, given the value f_i on the points of a stencil $S^{2r-1} = (x_{i-r+1}, ..., x_{i+r-1})$, the flux at any point can be evaluated as a $(2r-1)$-th order interpolating polynomial:

$$\hat{f}^{2r-1}(x) = f_i + \sum_{l=1}^{2(r-1)} a_l (x - x_i)^l. \tag{2.4}$$

Evaluating the function at the point $x_{i+\frac{1}{2}}$, the $(2r-1)$-th order approximation for $f_{i+\frac{1}{2}}$ is given by:

$$\hat{f}^L_{i+\frac{1}{2}} = q^{2r-1}(f_{i-r+1}, ..., f_{i+r-1}). \tag{2.5}$$

As is known in [9], the stencil S^{2r-1} can also be divided into r sub-stencils

$$S^{2r-1}_k = (x_{i+k-r+1}, x_{i+k-r+2}, ..., x_{i+k}), \qquad k = 0, 1, ..., r-1.$$

In each of these substencils, a r-th order approximation can be obtained

$$\hat{f}^{(k)}_{i+\frac{1}{2}} = q^r_k(f_{i+k-r+1}, ..., f_{i+k}) \tag{2.6}$$

where

$$q^r_k(g_0, ..., g_{r-1}) = \sum_{l=0}^{r-1} a^r_{k,l} g_l.$$

Here, $a^r_{k,l}$, $0 \le k, l \le r-1$, are constant coefficients.

The value $\hat{f}^L_{i+\frac{1}{2}}$ can also be obtained by a linear combination of $\hat{f}^{(k)}_{i+\frac{1}{2}}$

$$q^{2r-1}(f_{i-r+1}, ..., f_{i+r-1}) = \sum_{k=0}^{r-1} C^r_k q^r_k(f_{i+k-r+1}, ..., f_{i+k}). \tag{2.7}$$

The approximation (2.7) is linear. The resulted scheme can not capture strong shock waves and other discontinuities. Adopting the WENO idea, nonlinear weights ω_k^r are used to replace the linear weights C_k^r to obtain a nonlinear approximation

$$\hat{f}_{i+\frac{1}{2}} = \sum_{k=0}^{r-1} \omega_k^r q_k^r(f_{i+k-r+1}, ..., f_{i+k}) \tag{2.8}$$

where the nonlinear weight ω_k^r for the stencil S_k^{2r-1} is given by:

$$\omega_k^r = \frac{\alpha_k^r}{\alpha_0^r + \alpha_1^r + ... + \alpha_{r-1}^r} \tag{2.9}$$

with

$$\alpha_k^r = \frac{C_k^r}{(\varepsilon + IS_k^r)^p}, \qquad k = 0, 1, ..., r-1.$$

Here ε is a small positive number which is introduced to avoid the denominator becoming zero. We take $\varepsilon = 10^{-6}$ and the power $p = 2$ in this paper. IS_k is the smoothness indicator of the flux function in the *k-th* substencil which adopts the formulae given by Jiang and Shu [9] as:

$$IS_k^r = \sum_{l=1}^{r-1} \int_{x_{i-\frac{1}{2}}}^{x_{i+\frac{1}{2}}} \triangle x^{2l-1} \left(\frac{\partial^l f^{(r)}(x)}{\partial^l x} \right)^2 dx. \tag{2.10}$$

a. For $r = 3$

In the case of $r = 3$, the three third order numerical fluxes at the three substencils are given by

$$\begin{array}{l} \hat{f}_{j+1/2}^{(0)} = \frac{1}{8}(3f_{j-2} - 10f_{j-1} + 15f_j), \\ \hat{f}_{j+1/2}^{(1)} = \frac{1}{8}(-f_{j-1} + 6f_j + 3f_{j+1}), \\ \hat{f}_{j+1/2}^{(2)} = \frac{1}{8}(3f_j + 6f_{j+1} - f_{j+2}). \end{array} \tag{2.11}$$

The linear weights are given by

$$C_0^3 = \frac{1}{16}, \qquad C_1^3 = \frac{10}{16}, \qquad C_2^3 = \frac{5}{16}, \tag{2.12}$$

and the smoothness indicators are

$$\begin{array}{l} IS_0 = \frac{13}{12}(f_{j-2} - 2f_{j-1} + f_j)^2 + \frac{1}{4}(f_{j-2} - 4f_{j-1} + 3f_j)^2, \\ IS_1 = \frac{13}{12}(f_{j-1} - 2f_j + f_{j+1})^2 + \frac{1}{4}(f_{j-1} - f_{j+1})^2, \\ IS_2 = \frac{13}{12}(f_j - 2f_{j+1} + f_{j+2})^2 + \frac{1}{4}(3f_j - 4f_{j+1} + f_{j+2})^2. \end{array} \tag{2.13}$$

It is interesting that although there are differences between the WENO interpolation and the WENO reconstruction, they have the same smoothness indicators for the fifth order case. Since the nonlinear weights based on these smoothness indicators may lose accuracy at certain smooth extrema, Henrich et al. [8] introduced a mapping function as follows

$$g_r(\omega) = \frac{\omega(C_r + (C_r)^2 - 3C_r\omega + \omega^2)}{(C_r)^2 + (1 - 2C_r)\omega}, \tag{2.14}$$

where $\omega \in [0, 1]$ and $r = 0, 1, 2$. This function is monotonically increasing with a finite slope and $g_r(0) = 0$, $g_r(1) = 1$, $g_r(C_r) = C_r$, $g_r'(C_r) = 0$ and $g_r''(C_r) = 0$. The mapped weights are given by:

$$\omega_r^M = g_r(\omega_r), \tag{2.15}$$

where ω_r are computed by the equations (2.9) and (2.13). This mapped technique can improve accuracy at smooth extrema. An additional advantage is that accuracy depends much less on the magnitude of the parameter ε and hence it can be taken close to machine zero. We refer to [8] for more details.

Borges et al. [3] defined a new smoothness indicator given by

$$\beta_r^z = \frac{IS_r + \epsilon}{IS_r + \tau_5 + \epsilon}, \qquad r = 0, 1, 2 \tag{2.16}$$

where $\tau_5 = |IS_2 - IS_0|$, and the nonlinear weights are defined by

$$\omega_r^z = \frac{\alpha_r^z}{\sum_{l=0}^{2} \alpha_l^z}, \qquad \alpha_r^z = \frac{C_r}{\beta_r^z} = C_r \left(1 + \frac{\tau_5}{\beta_r + \epsilon}\right), \qquad r = 0, 1, 2. \tag{2.17}$$

With this new smoothness indicator, the improved scheme has similar accuracy at smooth extrema as the mapped technique, while the CPU cost is reduced by about 25%, since no mapping is necessary.

b. For $r = 4$

In the case of $r = 4$, the four fourth order numerical fluxes at the four substencils are

$$\begin{aligned}
\hat{f}^0_{i+\frac{1}{2}} &= \tfrac{1}{48}(-15f_{i-3} + 63f_{i-2} - 105f_{i-1} + 105f_i), \\
\hat{f}^1_{i+\frac{1}{2}} &= \tfrac{1}{48}(3f_{i-2} - 15f_{i-1} + 45f_i + 15f_{i+1}, \\
\hat{f}^2_{i+\frac{1}{2}} &= \tfrac{1}{48}(-3f_{i-1} + 27f_i + 27f_{i+1} - 3f_{i+2}), \\
\hat{f}^3_{i+\frac{1}{2}} &= \tfrac{1}{48}(15f_i + 45f_{i+1} - 15f_{i+2} + 3f_{i+3}).
\end{aligned} \tag{2.18}$$

The linear weights are given by

$$C_0^4 = \frac{1}{64}, \qquad C_1^4 = \frac{21}{64}, \qquad C_2^4 = \frac{35}{64}, \qquad C_3^4 = \frac{7}{64}. \tag{2.19}$$

The smoothness indicator are

$$\begin{aligned}
IS_0^4 = \;& f_{i-3}(79788 f_{i-3} - 566568 f_{i-2} + 680328 f_{i-1} - 273336 f_i) \\
& + f_{i-2}(1027692 f_{i-2} - 2523384 f_{i-1} + 1034568 f_i) \\
& + f_{i-1}(1610892 f_{i-1} - 1378728 f_i) + 308748 f_i^2, \\
IS_1^4 = \;& f_{i-2}(38028 f_{i-2} - 232488 f_{i-1} + 228168 f_i - 71736 f_{i+1}) \\
& + f_{i-1}(401292 f_{i-1} - 847224 f_i + 277128 f_{i+1}) \\
& + f_i(492012 f_i - 364968 f_{i+1}) + 79788 f_{i+1}^2, \\
IS_2^4 = \;& f_{i-1}(79788 f_{i-1} - 364968 f_i + 277128 f_{i+1} - 71736 f_{i+2}) \\
& + f_i(492012 f_i - 847224 f_{i+1} + 228168 f_{i+2}) \\
& + f_{i+1}(401292 f_{i+1} - 232488 f_{i+2}) + 38028 f_{i+2}^2, \\
IS_3^4 = \;& f_i(308748 f_i - 1378728 f_{i+1} + 1034568 f_{i+2} - 273336 f_{i+3}) \\
& + f_{i+1}(1610892 f_{i+1} - 2523384 f_{i+2} + 680328 f_{i+3}) \\
& + f_{i+2}(1027692 f_{i+2} - 566568 f_{i+3}) + 79788 f_{i+3}^2.
\end{aligned} \tag{2.20}$$

c. For $r = 5$

In the case of $r = 5$, the five fifth order numerical fluxes at the five substencils are

$$\begin{aligned}
\hat{f}^0_{i+\frac{1}{2}} &= \tfrac{1}{384}(105 f_{i-4} - 540 f_{i-3} + 1134 f_{i-2} - 1260 f_{i-1} + 945 f_i), \\
\hat{f}^1_{i+\frac{1}{2}} &= \tfrac{1}{384}(-15 f_{i-3} + 84 f_{i-2} - 210 f_{i-1} + 420 f_i + 105 f_{i+1}), \\
\hat{f}^2_{i+\frac{1}{2}} &= \tfrac{1}{384}(9 f_{i-2} - 60 f_{i-1} + 270 f_i + 180 f_{i+1} - 15 f_{i+2}), \\
\hat{f}^3_{i+\frac{1}{2}} &= \tfrac{1}{384}(-15 f_{i-1} + 180 f_i + 270 f_{i+1} - 60 f_{i+2} + 9 f_{i+3}), \\
\hat{f}^4_{i+\frac{1}{2}} &= \tfrac{1}{384}(105 f_i + 420 f_{i+1} - 210 f_{i+2} + 84 f_{i+3} - 15 f_{i+4}).
\end{aligned} \tag{2.21}$$

The linear weights are given by

$$C_0^5 = \frac{1}{256}, \qquad C_1^5 = \frac{9}{64}, \qquad C_2^5 = \frac{63}{128}, \qquad C_3^5 = \frac{21}{64}, \qquad C_2^5 = \frac{9}{256}. \tag{2.22}$$

The smoothness indicators are

$$
\begin{aligned}
IS_0 = \; & f_{i-4}(1114835f_{i-4} - 10262008f_{i-3} + 17985252f_{i-2} - 14254360f_{i-1} + 4301446f_i) \\
& + f_{i-3}(23768432f_{i-3} - 83962416f_{i-2} + 67148512f_{i-1} - 20460952f_i) \\
& + f_{i-2}(74964492f_{i-2} - 121605168f_{i-1} + 37653348f_i) \\
& + f_{i-1}(50449520f_{i-1} - 32188024f_i) + 5347091f_i^2, \\
IS_1 = \; & f_{i-3}(329267f_{i-3} - 2899576f_{i-2} + 4740132f_{i-1} - 3385432f_i + 886342f_{i+1}) \\
& + f_{i-2}(6595472f_{i-2} - 22176048f_{i-1} + 16196128f_i - 4311448f_{i+1}) \\
& + f_{i-1}(19389420f_{i-1} - 29385264f_i + 8042340f_{i+1}) \\
& + f_i(11710736f_i - 6846904f_{i+1}) + 1114835f_{i+1}^2, \\
IS_2 = \; & f_{i-2}(329267f_{i-2} - 2406328f_{i-1} + 3199908f_i - 1845208f_{i+1} + 393094f_{i+2}) \\
& + f_{i-1}(4914800f_{i-1} - 13983024f_i + 8404960f_{i+1} - 1845208f_{i+2}) \\
& + f_i(10783116f_i - 13983024f_{i+1} + 3199908f_{i+2}) \\
& + f_{i+1}(4914800f_{i+1} - 2406328f_{i+2}) + 329267f_{i+2}^2, \\
IS_3 = \; & f_{i-1}(1114835f_{i-1} - 6846904f_i + 8042340f_{i+1} - 4311448f_{i+2} + 886342f_{i+3}) \\
& + f_i(11710736f_i - 29385264f_{i+1} + 16196128f_{i+2} - 3385432f_{i+3}) \\
& + f_{i+1}(19389420f_{i+1} - 22176048f_{i+2} + 4740132f_{i+3}) \\
& + f_{i+2}(6595472f_{i+2} - 2899576f_{i+3}) + 329267f_{i+3}^2, \\
IS_4 = \; & f_i(5347091f_i - 32188024f_{i+1} + 37653348f_{i+2} - 20460952f_{i+3} + 4301446f_{i+4}) \\
& + f_{i+1}(50449520f_{i+1} - 121605168f_{i+2} + 67148512f_{i+3} - 14254360f_{i+4}) \\
& + f_{i+2}(74964492f_{i+2} - 83962416f_{i+3} + 17985252f_{i+4}) \\
& + f_{i+3}(23768432f_{i+3} - 10262008f_{i+4}) + 1114835f_{i+4}^2.
\end{aligned}
\tag{2.23}
$$

Taking the formulae of WENO interpolation into the physical flux $f_{i+\frac{1}{2}}$ of the equation (2.3), we can obtain WCNS schemes ranging from fourth order to ninth order accuracy.

2.2 Local characteristic projection for systems of conservative laws

For systems of conservation laws, such as the Euler equations (1.1), the procedure of the nonlinear WENO interpolation for the numerical fluxes $\hat{f}_{i+\frac{1}{2}}$ in the equations (2.8) and (2.10) are usually performed in the local characteristic fields, which is more robust in controlling spurious numerical oscillations. The procedure is as follows. Let $A_{i+\frac{1}{2}}$ be the Jacobian $\frac{dF}{dU}$ at the cell interface $x_{i+\frac{1}{2}}$, the left and right eigenvectors of $A_{i+\frac{1}{2}}$ are L_s and R_s. Then, the scalar WENO interpolation can be applied to each of the characteristic fields

$$\hat{f}^r_{i+\frac{1}{2},s} = L_s \sum_{j=0}^{k-1} c_{rj} f_{i-r+j}, \tag{2.24}$$

$$\hat{f}^{WENOI}_{i+\frac{1}{2},s} = \sum_{r=0}^{k-1} \omega^r_{k,s} \hat{f}^r_{i+\frac{1}{2},s}. \tag{2.25}$$

The nonlinear weights $\omega_{k,s}^r$ are also computed in the characteristic fields

$$\omega_{k,s}^r = \omega_k^r(L_s f_{i+k-r+1}, ..., L_s f_{i+k}). \tag{2.26}$$

When the WENO interpolation is finished in each characteristic field, the numerical fluxes obtained in the characteristic fields can then be projected back to the component space by

$$\hat{f}_{i+\frac{1}{2}}^{WENOI} = \sum_{s=1}^{m} \hat{f}_{i+\frac{1}{2},s}^{WENOI} R_s. \tag{2.27}$$

Traditionally, the Jacobian matrix $A_{i+\frac{1}{2}}$ is often computed by the Roe average [12] of the values of the numerical solution at the two neighboring points x_i and x_{i+1}. The Roe average for the Euler equations is given by

$$U_{i+\frac{1}{2}} = \frac{\rho_i}{\rho_i + \rho_{i+1}} U_i + \frac{\rho_{i+1}}{\rho_i + \rho_{i+1}} U_{i+1}, \tag{2.28}$$

where ρ is the density. Then the Jacobian matrix $A_{i+\frac{1}{2}}$ can be obtained by

$$A_{i+\frac{1}{2}} = A(U_{i+\frac{1}{2}}). \tag{2.29}$$

2.3 Flux splitting

The purpose of flux splitting is to introduce correct upwinding. In general, the flux can be split into two parts:

$$f(u) = f^+(u) + f^-(u), \tag{2.30}$$

where $\frac{df^+}{du} \geq 0$ and $\frac{df^-}{du} \leq 0$. The simplest and commonly used flux splitting is the Lax-Friedrichs flux splitting

$$f^{\pm}(u) = \frac{1}{2}(f(u) \pm \alpha u), \tag{2.31}$$

where $\alpha = \max |f'(u)|$ with the maximum taken over some relevant range of u.

2.4 Time discretization

After the spatial derivative is discretized with WCNS, we obtain a set of ordinary differential equations (ODEs):

$$\frac{du}{dt} = L(u). \tag{2.32}$$

The operator $L(u)$ is represented in (2.2). There are many methods that we can use to solve this set of ordinary differential equations. Implicit methods with suitable preconditioning, e.g. the methods in [18] are widely used, however there are issues related to extra numerical dissipation which need to be resolved. In this paper we adopt the explicit third order TVD Runge-Kutta method [15] to discretize the set of ordinary differential equations (2.2):

$$\begin{aligned} u^{(1)} &= u^n + \triangle t L(u^n), \\ u^{(2)} &= \tfrac{3}{4}u^n + \tfrac{1}{4}u^{(1)} + \tfrac{1}{4}\triangle t L(u^{(1)}), \\ u^{n+1} &= \tfrac{1}{3}u^n + \tfrac{2}{3}u^{(2)} + \tfrac{2}{3}\triangle t L(u^{(2)}). \end{aligned} \tag{2.33}$$

We remark that the simpler Euler forward time discretization is linearly unstable when coupled with high order WENO or WCNS spatial discretizations and should not be used.

3 The techniques to improve the convergence to steady state solutions for WCNS

In the previous section, we have given an overview of WCNS. WCNS is a high order shock capturing scheme and has been applied in many areas, especially for the flow over complex configuration [5]. However, like many other high order shock capturing schemes, it suffers from the convergence problem for the computation of steady state solutions [19]. In our previous work [21], we proposed a new smoothness indicator for the fifth order finite difference WENO scheme. With this new smoothness indicator, the residue of the fifth order WENO scheme for typical steady states can settle down to machine zero. However, in some critical points, this WENO scheme may lose accuracy. Based on extensive numerical tests, we found that the Roe average procedure to compute the Jacobian matrix $A_{i+\frac{1}{2}}$ may influence the convergence history of WENO schemes [20]. Instead of the Roe average, we used upwind biased interpolations to compute the physical variables at the middle point of a grid for the computation of the Jacobian matrix in [20]. The residue by this procedure can settle down to machine zero, while the accuracy is maintained. In this section, we generalize these two procedures to WCNS.

3.1 The new smoothness indicator

Based on a detailed analysis, we found that the second order term in the smoothness indicator for the fifth order WENO scheme is not adequate in the near region of a steady shock wave. Hence, in [21] we have removed the second order term and proposed a new smoothness indicator for the fifth order WENO scheme as follows

$$IS_r = 4 \int_{x_{j-\frac{1}{2}}}^{x_{j+\frac{1}{2}}} \triangle x \left(\frac{\partial p_r(x)}{\partial x} \right)^2 dx - \frac{1}{3} \int_{x_{j-\frac{1}{2}}}^{x_{j+\frac{1}{2}}} \triangle x^3 \left(\frac{\partial^2 p_r(x)}{\partial^2 x} \right)^2 dx. \tag{3.1}$$

The explicit formulae for this modified smoothness indicator are:

$$\begin{array}{l} IS_0 = (f_{j-2} - 4f_{j-1} + 3f_j)^2, \\ IS_1 = (f_{j-1} - f_{j+1})^2, \\ IS_2 = (3f_j - 4f_{j+1} + f_{j+2})^2. \end{array} \tag{3.2}$$

We can see from these explicit formulae that the modified smoothness indicators are always non-negative. We will use these modified smoothness indicators for the fourth and fifth order WCNS schemes to improve their steady state convergence.

3.2 Upwind biased interpolation

Instead of the Roe average, the physical variable $U_{i+\frac{1}{2}}$ at the cell interface can be obtained by the upwind biased interpolation [20]. For example, we can use zeroth order, first order one-sided interpolation and high order upwind-biased WENO interpolations (e.g. fifth order WENO interpolation for the fourth and fifth order WCNS, seventh order WENO interpolation for the sixth and seventh order WCNS and ninth order WENO interpolation for the eighth and ninth order WCNS). They are given as follows.

Zeroth order:

$$U^{(1)} = U_i, \qquad U^{(2)} = U_{i+1}. \tag{3.3}$$

First order:

$$U^{(1)} = (3U_i - U_{i-1})/2, \qquad U^{(2)} = (3U_{i+1} - U_{i+2})/2. \tag{3.4}$$

High order WENO interpolations: These are the same as that in the section 2 given by the formulae (2.7), (2.11), (2.18) and (2.21). For example,

$$\hat{U}^{(1)WENOI}_{i+\frac{1}{2}} = \sum_{r=0}^{k-1} \omega_k \hat{U}^k_{i+\frac{1}{2}} \tag{3.5}$$

where $\hat{U}^r_{i+\frac{1}{2}}$ is the lower order interpolation on each substencil given by

$$\hat{U}^k_{i+\frac{1}{2}} = \sum_{j=0}^{k-1} c_{kj} U_{i-k+j}. \tag{3.6}$$

Here, $U_{i+\frac{1}{2}} = U^{(1)}$ as $u_{i+\frac{1}{2}} \geq 0$ and $U_{i+\frac{1}{2}} = U^{(2)}$ when $u_{i+\frac{1}{2}} < 0$, where u denotes the velocity in the Euler equations.

4 Numerical experiments for the convergence to steady states of WCNS

4.1 One dimensional steady shock

One dimensional steady shock wave is a nice example to test the convergence of high order shock capturing scheme. In this example, there is no influence of boundary condition, which is also an important factor for the convergence of high order numerical schemes. This example has been used in our earlier papers [21, 20, 19] to test the convergence of WENO schemes [21, 20] and WCNS schemes [19]. The initial condition is given by the Rankine-Hugoniot relation [13]. We refer to our earlier papers [21, 19, 20] for more details. Figure 4.1 is the numerical density distribution along the computational domain obtained by the fourth order WCNS. We can see that the result is essentially non-oscillatory: no noticeable oscillations can be observed. The numerical shock profile is quite sharp and appears monotone to the eye. Figure 4.2 contains the zoomed density distribution (left) in the post shock region and the evolution of the average residue (right) for various WCNS schemes. In this figure, we use WCNS to represent the numerical result by the traditional weighted compact schemes, while WCNS4, WCNS5, WCNS6, WCNS7 and WCNS8 correspond the fourth, fifth, sixth, seventh and eighth order WCNS schemes, respectively. MWCNS represents the weighted compact scheme

combined with the mapped technique [8]. ZWCNS is the weighted compact scheme combined with the technique proposed by Borges et al. [3]. ZSWCNS is the weighted compact scheme combined with the new smoothness indicator proposed by Zhang and Shu [21]. U0WCNS, U1WCNS, and UWWCNS correspond the weighted compact scheme combined with zero order, first order and optimal weighted upwind biased interpolation for the physical variable in the cell interface. Based on this figure, we have the following observations: (1) There are relatively strong post-shock oscillations for the original WCNS schemes in the zoomed-in region and the residue can not settle down to machine zero but hangs at a relatively high level; (2) These relatively strong post-shock oscillations are totally removed by the use of either of the two techniques and the residue can settle down to machine zero for this test case. For the fourth order and fifth order WCNS schemes, the residue for all versions except WCNS and MWCNS can settle down to machine zero. This performance is quite similar to that in WENO schemes [20]. The physical variable from ZWCNS has a small overshoot after the shock wave. After considering the accuracy and the CPU cost, we recommend U0ZWCNS as the best choice. For higher order weighted compact schemes, it is interesting that the residue of U0WCNS and UWWCNS from sixth order to eighth order can settle down to machine zero, which are resulted from the removal of the strong post shock oscillation. Hence, the upwind biased interpolation is necessary for the higher order WCNS schemes.

4.2 135° oblique steady shock

As a two dimensional example, we simulate an oblique shock which has an angle of 135° with the positive x direction. The flow Mach number on the left of the shock is $M_\infty = 2$. The computational domain is $0 \leq x \leq 4$ and $0 \leq y \leq 2$. The initial oblique shock passes the point $(3, 0)$. The domain is divided into 200×100 equally spaced points with $\triangle x = \triangle y$.

Figure 4.3 contains the density contours obtained by the fourth order ZSWCNS. Figure 4.4 contains the evolution of the average residue by various fourth order (left) and fifth order (right) WCNS schemes. In the computation, the solution at the ghost points of the

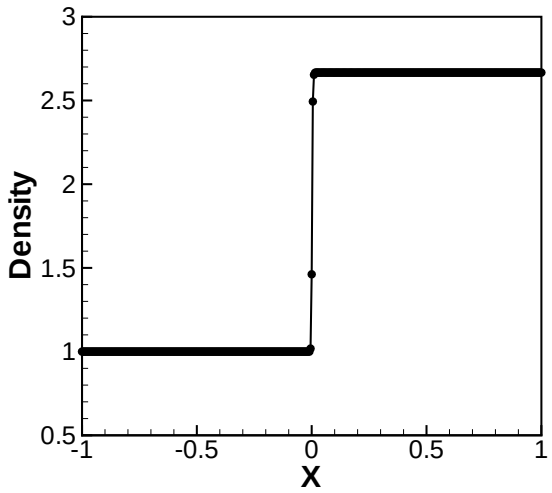

Figure 4.1: Density distribution around the one dimensional steady shock of $M_\infty = 2$ by the fourth order WCNS scheme.

upper and bottom boundaries is taken as the theoretical values that satisfy the Rankine-Hugoniot relation [13]. For this example, the residue can not settle down to machine zero. The residues obtained by the traditional fourth order weighted compact schemes are $10^{-2.39}$, $10^{-2.77}$ and $10^{-2.79}$ for WCNS4, MWCNS4 and ZWCNS4 respectively. The residues obtained by the traditional fifth order weighted compact schemes are $10^{-2.35}$, $10^{-2.80}$ and $10^{-1.88}$ for WCNS5, MWCNS5 and ZWCNS5 respectively. These values are quite high for steady state computation. With the new techniques of either the new smoothness indicator or the upwind biased interpolation for local characteristic decomposition, the convergence property is improved significantly. The best performance is obtained from the numerical scheme combining the usage of both the technique proposed by Borges et al. [3] and the zeroth order upwind biased interpolation. For example, the residue by U0ZWCNS4 can settle down to $10^{-7.8}$ and that of U0ZWCNS5 can settle down to $10^{-4.25}$. The residue from all other methods are much higher than those. Hence, it seems that the best method to use for the two dimensional case is the combination of the Z-technique and the upwind biased interpolation.

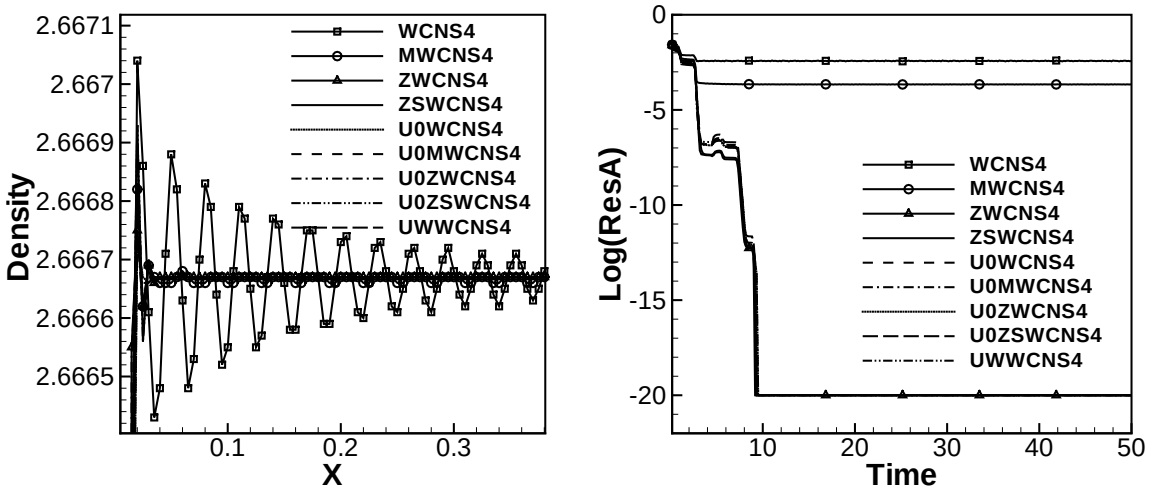

Fourth order WCNS

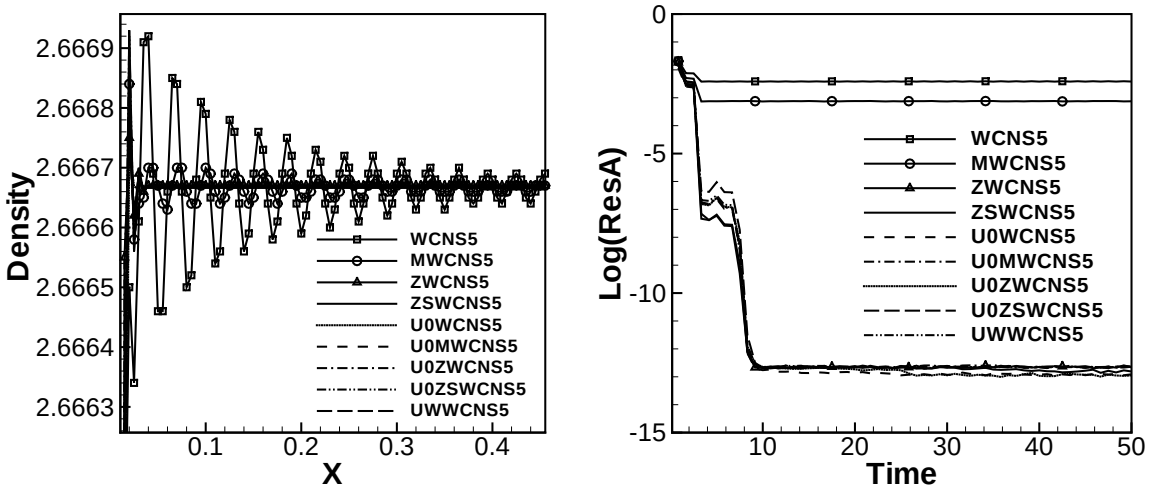

Fifth order WCNS

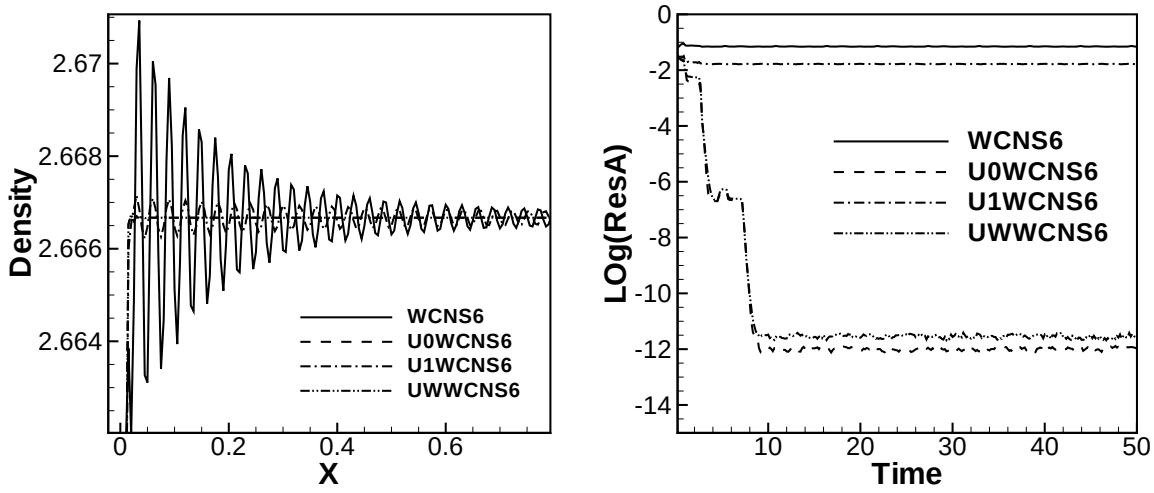

Sixth order WCNS

Figure 4.2: The zoomed density distribution (left) and the evolution of average residue (right) of the one dimensional steady shock of $M_\infty = 2$ by the WCNS schemes.

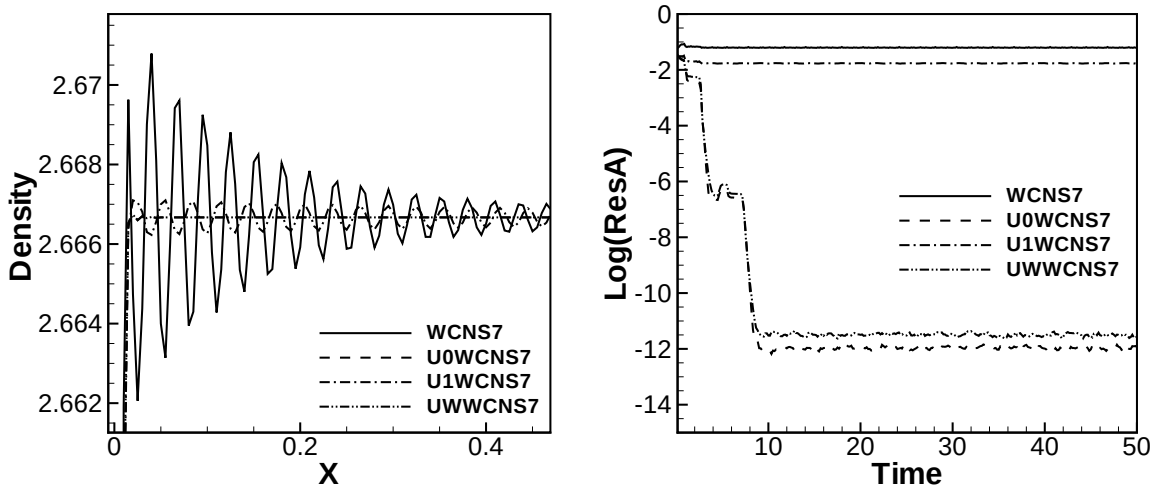

Seventh order WCNS

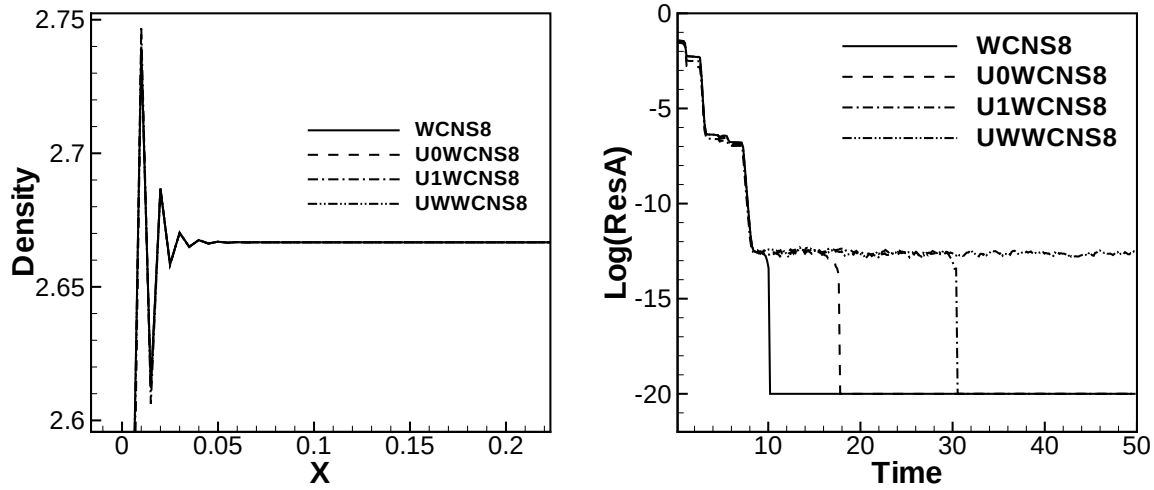

Eighth order WCNS

Figure 4.2: Continued.

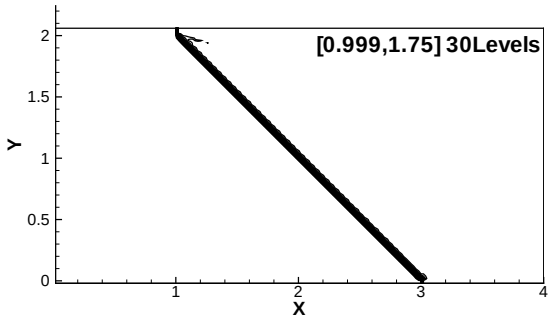

Figure 4.3: The density contour of a 135° oblique shock of $M_\infty = 2$ obtained by the fourth order ZSWCNS scheme.

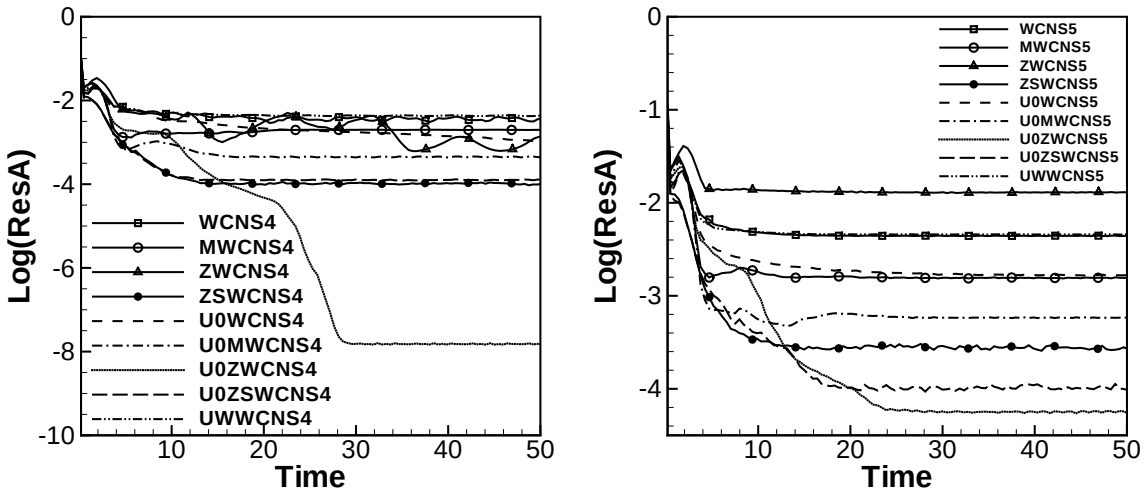

Figure 4.4: The evolution of the average residue for the 135° oblique shock. Left: Fourth order WCNS schemes; Right: Fifth order WCNS schemes.

5 Concluding remarks

The convergence to steady state solutions of the Euler equations for weighted compact schemes (WCNS) is studied through numerical experiments. Like most other shock capturing schemes, WCNS also suffers from the problem that the residue can not settle down to machine zero but hangs at a relatively high level for the steady state solutions containing shock waves. This problem is related to the appearance of slight post-shock oscillations.

In this paper, we test and compare the effect of our earlier introduced techniques to improve the convergence of WENO schemes [21, 20] on the WCNS schemes.

Numerical tests and comparison show that the relatively strong post-shock oscillations can be removed by the combination of two techniques. One is the high order smoothness indicator proposed by Borges et. al [3]. The other is the replacement of Roe average in the computation of Jacobian matrix in local characteristic decomposition by the zeroth order upwind biased interpolation [20]. The strong post-shock oscillation is removed and the residue can settle down to machine zero for typical one dimension cases, which has no boundary condition effect. For two dimensional oblique shock waves, which contain strong influence of boundary conditions since the oblique shock wave passes through the upper and

bottom boundaries, the convergence property is also improved significantly, although the residue cannot settle down to machine zero.

In comparison with the corresponding WENO schemes, the influence of boundary conditions on the convergence of WCNS seems to be more serious. This is perhaps due to the global influence through the banded linear solver in the compact schemes. This issue is left for our future study.

References

[1] Adams, N. A. and Shariff, K. (1996), A high-resolution hybrid compact-ENO scheme for shock-turbulence interaction problems. J. Comput. Phys. 127, 27-51.

[2] Balsara, D. S. and Shu, C.-W. (2000), Monotonicity preserving weighted essentially non-oscillatory schemes with increasingly high order of accuracy. J. Comput. Phys. 160, 405-452.

[3] Borges R., Carmona M., Costa B. and Don W.S. (2008), An improved weighted essentially non-oscillatory scheme for hyperbolic conservation laws. J. Comput. Phys. 227, 3191-3211.

[4] Colonius T. and Lele S.K. (2004), Computational aeroacoustics: progress on nonlinear problems of sound generation. Progress in Aerospace Sciences 40, 345-416.

[5] Deng X., Mao M., Tu G., Zhang Y. and Zhang H. (2010), Extending the fifth-order weighted compact nonlinear scheme to complex grids with characteristic-based interface conditions. AIAA J. 48, 2840-2851.

[6] Deng X. and Zhang H. (2000), Developing high-order weighted compact nonlinear schemes. J. Comput. Phys. 165, 22-44.

[7] Harten, A. Engquist, B. Osher, S. and Chakravarthy, S. (1987), Uniformly high order essentially non-oscillatory schemes, III. J. Comput. Phys. 71, 231-303.

[8] Henrick, A.K., Aslam, T. D. and Powers, J.M. (2005), Mapped weighted essentially non-oscillatory schemes: achieving optimal order near critical points. J. Comput. Phys. 207, 542-567.

[9] Jiang, G.-S. and Shu, C.-W. (1996), Efficient implementation of weighted ENO schemes. J. Comput. Phys. 126, 202-228.

[10] Lele, S.K. (1992), Compact finite difference schemes with spectral-like resolution. J. Comput. Phys. 103, 16-42.

[11] Liu, X.-D., Osher, S. and Chan, T. (1994), Weighted essentially non-oscillatory schemes, J. Comput. Phys. 115, 200-212.

[12] Roe, P.L. (1981), Approximate Riemann solvers, parameter vectors, and difference schemes. J. Comput. Phys. 43, 357-372.

[13] Saad, M.A. (1993), Compressible Fluid Flow, Prentice Hall.

[14] Sebastian, K. and Shu, C.-W. (2003), Multi domain WENO finite difference method with interpolation at subdomain interfaces, J. Sci. Comput. 19, 405-438.

[15] Shu, C.-W. and Osher, S. (1988), Efficient implementation of essentially non-oscillatory shock capturing schemes. J. Comput. Phys. 77, 439-471.

[16] Shu, C.-W. and Osher, S. (1989), Efficient implementation of essentially non- oscillatory shock capturing schemes II. J. Comput. Phys. 83, 32-78.

[17] Venkatakrishnan, V. (1995), Convergence to steady state solutions of the Euler equations on unstructured grids with limiters. J. Comput. Phys. 118, 120-130.

[18] Zhang L.P and Wang Z.J. (2004), A block LU-SGS implicit dual time-stepping algorithm for hybrid dynamic meshes. J. Comput. Phys. 33, 891-916.

[19] Zhang, S., Jiang, S. and Shu, C.-W. (2008), Development of nonlinear weighted compact schemes with increasingly higher order accuracy. J. Comput. Phys. 227, 7294-7321.

[20] Zhang, S., Jiang, S. and Shu, C.-W. (2011), Improvement of convergence to steady state solutions of Euler equations with the WENO schemes. J. Sci. Comput. 47, 216-238.

[21] Zhang, S. and Shu, C.-W. (2007), A new smoothness indicator for the WENO schemes and its effect on the convergence to steady state solution. J. Sci. Comput. 31, 273-305.

[22] Zhang, S., Zhang, H. and Shu, C.-W. (2009), Topological structure of shock induced vortex breakdown. Journal of Fluid Mech. 639, 343-372.

[23] Zhang, S., Zhang, Y.-T. and Shu, C.-W. (2005), Multistage interaction of a shock wave and a strong vortex. Phys. Fluid 17, 116101.